LEO Nadir-Pointing Attitude Stabilization via CLF–QP with Magnetorquers: Modeling, Controllability, and Receding-Horizon Synthesis

Ritwik Shankar
Dept. of Aerospace Engineering
Indian Institute of Technology Kanpur
Email: ritwik@iitk.ac.in

***Abstract*—I present a control framework for nadir-pointing attitude stabilization of a Low Earth Orbit (LEO) small satellite using only magnetorquers. The dynamics are formulated in quaternion coordinates with rigid-body rotational equations and magnetic actuation $\boldsymbol{\tau} = \mathrm{m} \times \mathbf{B}$. A Control Lyapunov Function (CLF) combining rotational kinetic energy and attitude error yields a convex *CLF–QP* at each step, enforcing $\dot{V} \leq -\alpha V$ subject to dipole saturation $\|\mathrm{m}\| \leq m_{\max}$. I extend this to a short-horizon MPC that incorporates the known future magnetic-field profile along a fixed orbit. Time-varying controllability over an orbit is analyzed via a Gramian built from $B_\times(t)$; observability assumptions and reachability limitations under saturation are discussed. Robustness is addressed by Gaussian process and measurement disturbances; feasibility is ensured via a slack variable. The framework is implementable in CasADi and supports later comparisons to LQR or discrete-time MPC linearizations in a unified state-space form. Planned simulations evaluate convergence rate, pointing accuracy, effort, and the impact of inclination and saturation.**

I. Introduction

The attitude control of Earth–orbiting spacecraft is central to maintaining sensor pointing, communication link alignment, and stability of platform operations. Modern small satellites, particularly nanosatellites and CubeSats, operate under stringent mass, poIr, and volume limitations that preclude the use of high–momentum actuators or propellant–based systems. Magnetic torque rods, or *magnetorquers*, which generate a magnetic dipole $\mathbf{m}$ interacting with Earth's geomagnetic field $\mathbf{B}$ to produce torque $\boldsymbol{\tau} = \mathbf{m} \times \mathbf{B}$, therefore remain one of the most attractive actuation mechanisms for low–cost missions due to their simplicity, reliability, and energy efficiency [**?**], [1], [2].

Despite these advantages, magnetic actuation is fundamentally underactuated because the torque can only be generated perpendicular to the ambient magnetic field direction. Consequently, instantaneous full three–axis control is impossible. HoIver, as a spacecraft orbits Earth, the magnetic field vector in the body frame varies quasi-periodically, enabling controllability over longer time horizons [3], [4]. This intrinsic time-varying structure has motivated both analytical and numerical control strategies ranging from linear time-varying (LTV) design to nonlinear adaptive schemes.

Early work on magnetic attitude control employed linearized small-angle models and periodic LQR design. Wisniewski [4] formulated the LTV equations for a nadir–pointing spacecraft in circular orbit and derived periodic gains ensuring asymptotic stability of small disturbances. Psiaki [3] later extended this framework to an asymptotic periodic LQR, demonstrating convergence of angular rates and Euler-angle errors over an orbit. While such linear controllers are computationally inexpensive, their validity is confined to near-nadir small-angle regimes and they cannot explicitly enforce actuator limits.

Nonlinear control approaches have since broadened the theoretical foundation for magnetorquer-only systems. Wang, Shtessel, and Wang [5] proposed a backstepping–based two-loop control structure dividing the dynamics into outer and inner subsystems in a geomagnetic reference frame. The outer loop regulated attitude using a virtual control input governed by LaSalle and Floquet stability theory, while the inner loop employed sliding-mode control to counter disturbances and guarantee asymptotic convergence. Their results verified that complete three-axis stabilization is attainable using only magnetic torquers, with distinct control phases for detumbling and attitude acquisition. Miyata and Van der Ha [6] further developed this idea by designing optimal periodic gains in the geomagnetic frame and validating them experimentally for small satellites, confirming the practicality of magnetic-only actuation in LEO.

Complementary studies explored Lyapunov–based and passivity–based designs. Silani and Lovera [2] analyzed stability and performance trade-offs of nonlinear feedback laws under time-varying $\mathbf{B}$, introducing a global Lyapunov function to study the energy dissipation properties of magnetic control. Other authors introduced adaptive and disturbance-observer–based laws to mitigate model uncertainty and environmental torques [7], [8]. Collectively, these efforts demonstrated that magnetic control can ensure stability and near-nadir alignment, though convergence speed and robustness remain limited by the slowly varying nature of the geomagnetic

vector.

Recent advances in nonlinear and optimization-based control have opened new perspectives. Model Predictive Control (MPC) enables the inclusion of actuator saturation and horizon-based anticipation of the field variation, while maintaining real-time implementability for low-order spacecraft models. The Control Lyapunov Function (CLF) framework, introduced by Ames et al. for robotic systems [9], provides a mathematically rigorous method to embed Lyapunov stability conditions directly into a convex Quadratic Program (QP). By ensuring the inequality

$$L_f V(x) + L_g V(x)\,\mathbf{m} \leq -\alpha V(x), \tag{1}$$

the controller enforces a guaranteed rate of decrease of a Lyapunov function $V(x)$ while minimizing control effort subject to physical constraints. The same idea can be extended to a receding-horizon (MPC-CLF) formulation, combining predictive optimization with provable stability.

In the context of spacecraft attitude control, the CLF–QP paradigm offers several advantages:

- It preserves nonlinear quaternion kinematics, avoiding singularities inherent in Euler-angle formulations.
- It handles actuator saturation $\|\mathbf{m}\| \leq m_{\max}$ and magnetic torque orthogonality constraints explicitly.
- It unifies Lyapunov stability analysis with optimization, yielding a convex QP solvable in milliseconds on embedded processors using solvers such as OSQP or qpOASES.
- It naturally accommodates noise, disturbances, and time-varying field models through slack variables and robustness margins.

This project applies the CLF–QP approach to a **Low Earth Orbit (LEO) nadir-pointing satellite**, using magnetorquers as the sole actuators. The orbital path and magnetic field profile are assumed known, allowing prediction of $\mathbf{B}(t)$ over a finite horizon. The dynamics are derived from the rigid-body model presented by De Ruiter, Damaren, and Forbes [1], expressed in quaternion form and embedded in a control-affine structure. The control objective is formulated as a convex QP ensuring the Lyapunov decrease condition (1) while minimizing dipole effort. The design incorporates a receding-horizon extension, controllability and reachability analysis following the magnetic-field Gramian formulation [2], and robustness tests under Gaussian disturbances.

The remainder of this report is organized as follows. Section II formulates the satellite dynamics in quaternion representation with magnetic torque modeling and coordinate transformations among the inertial, orbital, and body frames. Section III introduces the CLF design and QP formulation, folloId by the receding-horizon predictive control structure. Section IV examines controllability, observability, and reachability conditions for magnetic actuation. Section V presents stability and robustness analysis, while Section VI outlines the simulation framework and performance metrics. Conclusions and directions for future work are given in Section VII.

Contributions

- Full symbolic quaternion dynamics with magnetic actuation and body/inertial frame mappings.
- CLF construction and *per-step* convex QP with optional slack for feasibility.
- Receding-horizon formulation that anticipates $\mathbf{B}(t)$ along a fixed orbit.
- Controllability over an orbit via a $B_\times$-based Gramian; observability and reachability discussion.
- Robustness to Gaussian disturbances and measurement noise; saturation handling.
- State-space linearization pathway for LQR and discrete MPC baselines.

II. Problem Statement

Goal: Achieve nadir pointing in LEO with magnetorquers only. Denote state $x = [\boldsymbol{\omega}^\top, q^\top]^\top$, where $\boldsymbol{\omega} \in \mathbb{R}^3$ is body-frame angular velocity and $q = [q_0, \mathbf{q}_v^\top]^\top \in \mathbb{S}^3$ is the unit quaternion. The desired attitude $q_d(t)$ aligns body $-z$ with Earth center and x with along-track, i.e., tracks the LVLH frame.

Control input: magnetic dipole $\mathbf{m} \in \mathbb{R}^3$ with bound $\|\mathbf{m}\| \leq m_{\max}$ (or per-axis bounds). Torque is $\boldsymbol{\tau} = \mathbf{m} \times \mathbf{B}$ in body coordinates.

Disturbances/noise: additive torque $\boldsymbol{\tau}_d$; measurement noise on attitude and rate. Both are modeled as Gaussian in simulation.

Objectives:

1) Stabilize $(\tilde{q}, \boldsymbol{\omega}) \to ((1, \mathbf{0}), \mathbf{0})$ where $\tilde{q} = q_d^{-1} \otimes q$.
2) Enforce actuator saturation and minimize control effort.
3) Provide stability guarantees via CLF and analyze robustness.

III. Satellite Model

This section fixes geometry, frames, attitude representations, rigid-body dynamics, and the magnetorquer actuator model used later for CLF–QP synthesis and MPC prediction. I adopt an Earth-centered inertial (ECI) frame $\{\mathcal{I}\}$, a body-fixed frame $\{\mathcal{B}\}$ attached to the spacecraft, and a local-vertical local-horizontal (LVLH) frame $\{\mathcal{L}\}$ for nadir pointing along the reference low-Earth orbit; see Figs. 1 and 2.

A. Geometry and Frames

Spacecraft description. I follow the characterized microsatellite model: mass $m = 17.7$ kg, undeployed dimensions $200 \times 200 \times 200$ mm, three orthogonal magnetorquers aligned with the nominal principal axes, and deployable solar wings that can alter the inertia tensor (used later only for parametric studies) [10].[1]

Let $C_{\mathcal{I}}^{\mathcal{B}} \in \mathbb{R}^{3\times3}$ be the direction–cosine matrix (DCM) mapping inertial vectors to the body frame. For any inertial vector $v_{\mathcal{I}}$, $v_{\mathcal{B}} = C_{\mathcal{I}}^{\mathcal{B}} v_{\mathcal{I}}$. I will realize $C_{\mathcal{I}}^{\mathcal{B}}$ either as a 3–2–1 Euler DCM or via a quaternion–to–DCM map and reference these in (2) and (3).

[1]Exact numerical inertia entries are not required in this section; I denote the body inertia by $I \in \mathbb{R}^{3\times3}$. See Sec. III-C for usage.

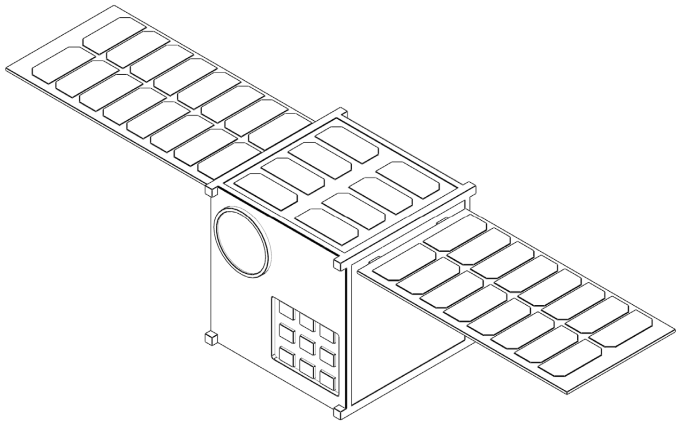

Fig. 1: Characterized satellite model.

B. Attitude Representations: C_{321} and C_q

3–2–1 Euler DCM. With yaw–pitch–roll (ψ, θ, ϕ), the 3–2–1 DCM is

$$C_{321}(\phi,\theta,\psi) = \begin{bmatrix} \cos\theta\cos\psi & \cos\theta\sin\psi & -\sin\theta \\ -\cos\phi\sin\psi + \sin\phi\sin\theta\cos\psi & \cos\phi\cos\psi + \sin\phi\sin\theta\sin\psi & \sin\phi\cos\theta \\ \sin\phi\sin\psi + \cos\phi\sin\theta\cos\psi & -\sin\phi\cos\psi + \cos\phi\sin\theta\sin\psi & \cos\phi\cos\theta \end{bmatrix} \tag{2}$$

Quaternion DCM. For a unit quaternion $q = [q_0\ q_1\ q_2\ q_3]^\top$ (scalar-first), the equivalent DCM is

$$C_q(q) = \begin{bmatrix} q_0^2+q_1^2-q_2^2-q_3^2 & 2(q_1q_2+q_0q_3) & 2(q_1q_3-q_0q_2) \\ 2(q_1q_2-q_0q_3) & q_0^2-q_1^2+q_2^2-q_3^2 & 2(q_2q_3+q_0q_1) \\ 2(q_1q_3+q_0q_2) & 2(q_2q_3-q_0q_1) & q_0^2-q_1^2-q_2^2+q_3^2 \end{bmatrix} \tag{3}$$

For geomagnetic computations I use $C_{\mathcal{I}}^{\mathcal{B}} = C_q(q)$ so the Earth magnetic field maps as

$$b_{\mathcal{B}}(t) = C_q(q(t))\, b_{\mathcal{I}}(t), \tag{4}$$

which I will reference repeatedly in the control synthesis.

C. Rigid-Body Attitude Dynamics

The rotational dynamics in $\{\mathcal{B}\}$ follow Euler's equation with magnetic actuation:

$$I\dot{\omega} = -\,\omega \times (I\omega) + \tau_{\text{mtq}} + \tau_{\text{dist}}, \tag{5}$$

where $\omega \in \mathbb{R}^3$ is the body angular rate, τ_{mtq} is the magnetorquer torque from (7), and τ_{dist} collects environmental and unmodeled torques. The state I simulate later is $x = [\,q^\top\ \omega^\top\,]^\top$ with $\|q\| = 1$.

D. Magnetorquer Actuator Model

Each orthogonal air-core coil produces a dipole

$$m = i\, n\, S\, \hat{u}, \tag{6}$$

with current i, turns $n = 250$, area $S = 3.497 \times 10^{-2}\,\text{m}^2$, and unit axis $\hat{u}$ fixed in $\{\mathcal{B}\}$. The torque law is the magnetic cross product

$$\tau_{\text{mtq}} = m \times b_{\mathcal{B}}. \tag{7}$$

Hardware bounds and a measured calibration imply $\|m\| \le 8.19\,\text{A}{\cdot}\text{m}^2$ at $i = 0.92$ A and coil resistance $R = 9.7\,\Omega$; per-axis dipole saturation will be enforced in the controller [**?**].

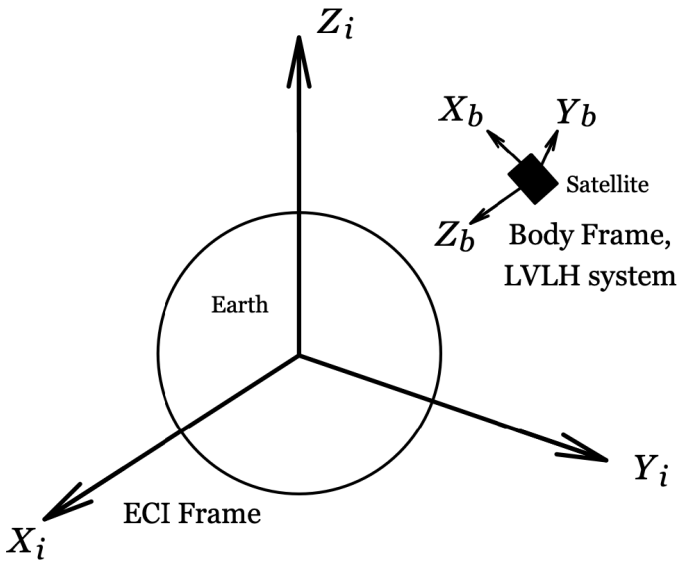

Fig. 2: ECI $\{\mathcal{I}\}$, body $\{\mathcal{B}\}$, and LVLH $\{\mathcal{L}\}$ frames for nadir pointing.

E. Assumptions, Saturations, and Noises

Saturations. Currents satisfy $i \in [-i_{\max}, i_{\max}]$, giving $\|m\| \le m_{\max} = nS\, i_{\max}$; thus $\|\tau_{\text{mtq}}\| \le \|m\|\,\|b_{\mathcal{B}}\|$ by (7).

Disturbances and sensors. I use white gaussian noise as our small sensor noise model, more specifcially I use $\tau_{\text{dist}} = \tau_{\text{env}} + w_\tau$, with $w_\tau \sim \mathcal{N}(0, \Sigma_\tau)$, a magnetometer $\tilde{b}_{\mathcal{B}} = b_{\mathcal{B}} + \eta_b$, and a gyro $\tilde{\omega} = \omega + \eta_\omega$, where $\eta_b \sim \mathcal{N}(0, \Sigma_b)$ and $\eta_\omega \sim \mathcal{N}(0, \Sigma_\omega)$. These enter the estimator and robust CLF–QP design later.

IV. Frames and Reference Attitudes

I use three frames: inertial ECI $\{\mathcal{I}\}$, local-vertical local-horizontal (LVLH/RSW) $\{\mathcal{L}\}$, and body $\{\mathcal{B}\}$. The orbit is maintained by an external controller; I only design attitude. Let $\mathbf{r}, \mathbf{v}$ be the ECI position and velocity. Define the LVLH triad

$$\hat{\mathbf{R}} = \frac{\mathbf{r}}{\|\mathbf{r}\|}, \qquad \hat{\mathbf{W}} = \frac{\mathbf{r}\times\mathbf{v}}{\|\mathbf{r}\times\mathbf{v}\|}, \qquad \hat{\mathbf{S}} = \hat{\mathbf{W}} \times \hat{\mathbf{R}}, \tag{8}$$

and the DCM $C_{\mathcal{I}}^{\mathcal{L}} = [\hat{\mathbf{R}}\ \hat{\mathbf{S}}\ \hat{\mathbf{W}}]^\top$ so $\mathbf{a}_{\mathcal{L}} = C_{\mathcal{I}}^{\mathcal{L}}\mathbf{a}_{\mathcal{I}}$ [1].

a) Nadir/along-track pointing map.: The nadir-pointing requirement is $-\mathbf{z}_{\mathcal{B}} \parallel \hat{\mathbf{R}}$ with $\mathbf{x}_{\mathcal{B}} \parallel \hat{\mathbf{S}}$. A constant body-to-LVLH alignment that satisfies this is

$$C_{\mathcal{L}}^{\mathcal{B}} = \begin{bmatrix} 0 & 1 & 0 \\ 0 & 0 & -1 \\ -1 & 0 & 0 \end{bmatrix}, \qquad C_{\mathcal{I},\text{des}}^{\mathcal{B}}(t) = C_{\mathcal{L}}^{\mathcal{B}}\, C_{\mathcal{I}}^{\mathcal{L}}(t). \tag{9}$$

The desired quaternion is $q_d(t) = \text{DCM2Quat}(C_{\mathcal{I},\text{des}}^{\mathcal{B}}(t))$. If a mission requires a yaw bias $\psi_y(t)$ about $-\hat{\mathbf{R}}$, I insert $R_{\mathcal{L}}(\psi_y)$ between $C_{\mathcal{L}}^{\mathcal{B}}$ and $C_{\mathcal{I}}^{\mathcal{L}}$.

b) Future reference quaternions.: The receding-horizon controller uses predicted reference attitudes $\{q_{d,k}\}_{k=0}^{N}$ over a horizon N. I can obtain $q_{d,k}$ (i) directly from a supplied

attitude timeline in $\{\mathcal{I}\}$, or (ii) from a supplied ground-track/ephemeris by building $C_{\mathcal{I}}^{\mathcal{L}}(t_k)$ with (8) and then using (9). Both are consistent with nadir pointing in LEO [1].

c) Magnetic-field mapping.: Given $\mathbf{B}_{\mathcal{I}}(t)$ from an IGRF/dipole model, the body-field used for actuation is

$$\mathbf{B}_{\mathcal{B}}(t) = C_{\mathcal{I}}^{\mathcal{B}}(q(t))\,\mathbf{B}_{\mathcal{I}}(t), \qquad \boldsymbol{\tau}_{\mathrm{mtq}} = \mathbf{m} \times \mathbf{B}_{\mathcal{B}}. \tag{10}$$

Time-variation of $\mathbf{B}_{\mathcal{B}}$ across an orbit underpins magnetic controllability [2], [3].

V. Mathematical Modeling and Receding-Horizon CLF–QP Formulation

A. States, kinematics, and dynamics

I use the quaternion $q = [q_0,\ \mathbf{q}_v^\top]^\top$ (scalar-first) and body rate $\boldsymbol{\omega} \in \mathbb{R}^3$. The kinematics and rigid-body dynamics are

$$\dot{q} = \tfrac{1}{2}\,W(q)\,\boldsymbol{\omega}, \qquad W(q) = \begin{bmatrix} -q_1 & -q_2 & -q_3 \\ q_0 & -q_3 & q_2 \\ q_3 & q_0 & -q_1 \\ -q_2 & q_1 & q_0 \end{bmatrix}, \tag{11}$$

$$I\dot{\boldsymbol{\omega}} = -\boldsymbol{\omega} \times (I\boldsymbol{\omega}) \ + \ \underbrace{\mathbf{m} \times \mathbf{B}_{\mathcal{B}}}_{\boldsymbol{\tau}_{\mathrm{mtq}}} + \boldsymbol{\tau}_{\mathrm{dist}}, \tag{12}$$

with I the body inertia. Control is the magnetic dipole $\mathbf{m} \in \mathbb{R}^3$ subject to bounds $\|\mathbf{m}\|_\infty \le m_{\max}$ (coil limits). The stacked state is $x = [q^\top,\ \boldsymbol{\omega}^\top]^\top$.

a) Error quaternion and rates.: At sample k, define the right-invariant error quaternion

$$\tilde{q}_k = q_{d,k}^{-1} \otimes q_k, \qquad \tilde{q}_k = [\tilde{q}_{0,k},\ \tilde{\mathbf{q}}_{v,k}^\top]^\top, \tag{13}$$

and the body rate error $\tilde{\boldsymbol{\omega}}_k = \boldsymbol{\omega}_k - \boldsymbol{\omega}_{d,k}$, with $\boldsymbol{\omega}_{d,k}$ the (optional) desired body rate induced by $q_{d,k}$. For nadir pointing I typically set $\boldsymbol{\omega}_{d,k} = \mathbf{0}$.

B. Discretization for prediction

With step Δt, I use a first-order discrete model suitable for QP:

$$\begin{aligned} x_{k+1} &= f_d(x_k, \mathbf{m}_k) \\ &= \begin{bmatrix} q_k + \frac{\Delta t}{2}\,W(q_k)\,\boldsymbol{\omega}_k \\ \boldsymbol{\omega}_k + \Delta t\, I^{-1}\Big(-\boldsymbol{\omega}_k \times (I\boldsymbol{\omega}_k) + \mathbf{m}_k \times \mathbf{B}_{\mathcal{B},k}\Big) \end{bmatrix}, \end{aligned} \tag{14}$$

followed by quaternion renormalization $q_{k+1} \leftarrow q_{k+1}/\|q_{k+1}\|$. For a convex QP I include the state trajectory $\{x_k\}$ as decision variables and enforce (14) as *linearized* equality constraints about a nominal $(\bar{x}_k, \bar{\mathbf{m}}_k)$:

$$x_{k+1} \approx A_k\,x_k + B_k\,\mathbf{m}_k + c_k, \quad B_k = \Delta t \begin{bmatrix} \mathbf{0}_{4\times 3} \\ I^{-1}\,[\mathbf{B}_{\mathcal{B},k}]_\times \end{bmatrix}, \tag{15}$$

where $[\cdot]_\times$ is the skew map and A_k, c_k come from Jacobians of (14). This keeps the program quadratic and convex.

C. Control Lyapunov Function and decay condition

I adopt the CLF

$$V(x_k) = \tfrac{1}{2}\,\boldsymbol{\omega}_k^\top I\,\boldsymbol{\omega}_k + \tfrac{\kappa}{2}\,\|\tilde{\mathbf{q}}_{v,k}\|^2, \qquad \kappa > 0, \tag{16}$$

whose continuous-time derivative (nominal, without disturbances) is

$$\dot{V} = (\mathbf{B}_{\mathcal{B}} \times \boldsymbol{\omega})^\top \mathbf{m} + \tfrac{\kappa\,\tilde{q}_0}{2}\,\tilde{\mathbf{q}}_v^\top \boldsymbol{\omega}. \tag{17}$$

The CLF decay inequality

$$(\mathbf{B}_{\mathcal{B},k} \times \boldsymbol{\omega}_k)^\top \mathbf{m}_k \ \le\ -\alpha V(x_k) - \tfrac{\kappa\,\tilde{q}_{0,k}}{2}\,\tilde{\mathbf{q}}_{v,k}^\top \boldsymbol{\omega}_k + \delta_k, \tag{18}$$

with $\alpha > 0$ and slack $\delta_k \ge 0$, is *affine* in $\mathbf{m}_k$ and therefore QP-compatible [9]. I penalize δ_k heavily to preserve feasibility under adverse $\mathbf{B}$ alignments.

a) Computing $\dot{V}$.: Using (12) and $\dot{\tilde{\mathbf{q}}}_v = \frac{1}{2}\big(\tilde{q}_0 I_3 + [\tilde{\mathbf{q}}_v]_\times\big)\boldsymbol{\omega} - \frac{1}{2}\big(\tilde{q}_0 I_3 + [\tilde{\mathbf{q}}_v]_\times\big)\boldsymbol{\omega}_d$ (with $\boldsymbol{\omega}_d = \mathbf{0}$ here), the nominal derivative is

$$\begin{aligned} \dot{V} &= \boldsymbol{\omega}^\top\Big(-\boldsymbol{\omega} \times (I\boldsymbol{\omega}) + \mathbf{m} \times \mathbf{B}_{\mathcal{B}}\Big) \ + \ \kappa\,\tilde{\mathbf{q}}_v^\top \dot{\tilde{\mathbf{q}}}_v \\ &= (\mathbf{B}_{\mathcal{B}} \times \boldsymbol{\omega})^\top \mathbf{m} \ + \ \tfrac{\kappa\,\tilde{q}_0}{2}\,\tilde{\mathbf{q}}_v^\top \boldsymbol{\omega}. \end{aligned} \tag{19}$$

The gyroscopic power term $\boldsymbol{\omega}^\top\big(-\boldsymbol{\omega} \times (I\boldsymbol{\omega})\big) = 0$ by skew-symmetry. The first term in (19) is the control channel $L_g V$ (bilinear in $\mathbf{m}$ via $\mathbf{B}_{\mathcal{B}} \times \boldsymbol{\omega}$); the second is the natural kinematic coupling $L_f V$ from attitude error to rate.

b) Why enforce $\dot{V} \le -\alpha V$.: If $\dot{V} \le -\alpha V$ with $\alpha > 0$, then $V(t) \le e^{-\alpha t} V(0)$: the energy-like measure V decays exponentially, which implies $\tilde{\mathbf{q}}_v \to 0$ and $\boldsymbol{\omega} \to 0$ (global except for the quaternion sign ambiguity) [9]. This gives a *formal stability guarantee* under actuator limits when the inequality is enforced by the controller rather than assumed in analysis. In practice the magnetic channel may be weak or momentarily unaligned (e.g., $\mathbf{B}_{\mathcal{B}}$ nearly collinear with $\boldsymbol{\omega}$), so I introduce a nonnegative slack δ to maintain feasibility; then $\dot{V} \le -\alpha V + \delta$ yields the bound

$$V(t) \le e^{-\alpha t} V(0) + \tfrac{1 - e^{-\alpha t}}{\alpha}\,\bar{\delta},$$

i.e., *practical* exponential stability to a ball set by the worst-case slack $\bar{\delta}$. Penalizing δ in the cost shrinks this ball.

c) Affine decay constraint used in the QP.: Discretizing (19) stage-wise and upper-bounding $\dot{V}$ by its sample value gives the convex, control-affine inequality

$$(\mathbf{B}_{\mathcal{B},k} \times \boldsymbol{\omega}_k)^\top \mathbf{m}_k \ \le\ -\alpha V(x_k) - \tfrac{\kappa\,\tilde{q}_{0,k}}{2}\,\tilde{\mathbf{q}}_{v,k}^\top \boldsymbol{\omega}_k + \delta_k, \tag{20}$$

where every term is known at sample k except $\mathbf{m}_k$ and the slack $\delta_k \ge 0$.

- $(\mathbf{B}_{\mathcal{B},k} \times \boldsymbol{\omega}_k)^\top \mathbf{m}_k$ is the controllable decrease rate; it vanishes if $\mathbf{m}_k \parallel \mathbf{B}_{\mathcal{B},k}$ and is maximized when $\mathbf{m}_k$ aligns with $\mathbf{B}_{\mathcal{B},k} \times \boldsymbol{\omega}_k$.
- $-\alpha V(x_k)$ sets the desired contraction rate; larger α yields faster convergence but requires larger dipoles and may be infeasible under saturation.
- $-\frac{\kappa\,\tilde{q}_{0,k}}{2}\,\tilde{\mathbf{q}}_{v,k}^\top \boldsymbol{\omega}_k$ compensates the uncontrolled kinematic power injection.

- δ_k prevents infeasibility (e.g., $\|\mathbf{B}_{\mathcal{B},k}\|$ small) and is quadratically penalized.

This is the standard CLF–QP construction specialized to magnetic actuation [9], [1], [2].

D. Receding-horizon CLF–QP

I stack decision variables $z = \{\, x_k, \mathbf{m}_k, \delta_k \,\}_{k=0}^{N-1} \cup \{x_N\}$ and solve

$$\min_{z} \quad \sum_{k=0}^{N-1} \left(\tfrac{1}{2}\|\mathbf{m}_k\|^2 + \rho\, \delta_k^2 \right) \;+\; \lambda V(x_N) + \sum_{k=0}^{N} \tfrac{1}{2}\, x_k^\top Q x_k \tag{21}$$

$$\text{s.t.} \quad x_{k+1} = A_k x_k + B_k \mathbf{m}_k + c_k, \quad k = 0{:}N-1, \tag{22}$$

$$(\mathbf{B}_{\mathcal{B},k} \times \boldsymbol{\omega}_k)^\top \mathbf{m}_k \le -\alpha V(x_k) - \tfrac{\kappa \tilde{q}_{0,k}}{2} \tilde{\mathbf{q}}_{v,k}^\top \boldsymbol{\omega}_k + \delta_k, \tag{23}$$

$$-\, m_{\max} \le (m_k)_i \le m_{\max}, \quad i = 1,2,3, \;\; k = 0{:}N-1, \tag{24}$$

$$\delta_k \ge 0, \quad k = 0{:}N-1. \tag{25}$$

Here $Q \succeq 0$ regularizes the state, $\lambda \ge 0$ imposes a terminal CLF weight, and $\rho \gg 1$ penalizes CLF violations. The equality constraints (22) are from (15). Constraint (23) enforces Lyapunov decrease stage-wise, guaranteeing stability while respecting actuation limits (24). I apply only $\mathbf{m}_0^\star$, shift the horizon, update q_d and $\mathbf{B}_\mathcal{B}$, and resolve.

a) Variant: single-step CLF–QP (feedback).: For $N = 1$ and $Q = \lambda = 0$, (21)–(25) reduce to the per-step CLF–QP

$$\min_{\mathbf{m},\delta \ge 0} \;\; \tfrac{1}{2}\|\mathbf{m}\|^2 + \rho\delta^2 \;\text{s.t.}\; (\mathbf{B}_\mathcal{B} \times \boldsymbol{\omega})^\top \mathbf{m} \le -\alpha V - \tfrac{\kappa \tilde{q}_0}{2} \tilde{\mathbf{q}}_v^\top \boldsymbol{\omega} + \delta,$$

which I use as a fallback when computation is tight.

E. Notes on frames inside the optimization

All field terms are built from (10). The reference $q_{d,k}$ is formed by (9) from ephemerides (or taken directly if provided in $\{\mathcal{I}\}$). Error states (13) enter the CLF (16). Dynamics use body-frame $\boldsymbol{\omega}$ and torques (12); the input map in the linearization has the analytic form B_k in (15). This separation keeps the QP convex while preserving the multi-frame geometry emphasized in this course [1], [2], [3], [9].

F. Saturation, disturbances, and noise

I enforce per-axis dipole bounds via (24). Disturbance torques are injected in (12) during simulation; the slack δ_k provides robustness to modeling errors and $\mathbf{B}$ nulls. Sensor noise enters through the estimator that supplies $(q_k, \boldsymbol{\omega}_k)$; the QP uses those estimates directly.

Outcome. The formulation (21)–(25) generates a sequence of dipoles that steers the spacecraft from its current attitude to the desired nadir-pointing attitude over a receding horizon, while guaranteeing Lyapunov decrease and respecting magnetic actuation constraints.

G. Magnetorquer Hardware Used

I adopt a three–axis, square, air–core magnetorquer set whose parameters were experimentally characterized and validated using Biot–Savart modeling and bench measurements with a Group3 DTM-130 teslameter (0–15 V sweep) completely inspired by the work of T. Panyalert et al [10]. The authors report an average magnetic-field intensity error of $\approx$1.26% across 0–120 mm, confirming model–measurement agreement suitable for control design

a) Actuation principle.: Control torque is generated by the magnetic cross product

$$\tau_{\mathrm{mtq}} = m \times B, \tag{26}$$

where m is the coil dipole moment and B is the geomagnetic field expressed in the same frame.

b) Implemented hardware parameters.: The key coil specifications used in our simulations are taken from the characterization study's [10] Table 2 (single-axis values; three orthogonal coils provide full 3-axis actuation) and are presented in Table I.

TABLE I: Magnetorquer parameters adopted from the characterization study.

Quantity	Value
Geometry (square coil)	$200 \times 200 \times 10$ mm
Turns	250
Wire	AWG22 Cu, diameter 0.6426 mm
Effective area	3.497×10^{-2} m^2
Resistance	9.7 Ω
Max current (tested)	0.92 A (supply limited)
Max dipole @ 0.92 A	8.19 A m^2
Mass	637.8 g
Calibration method	Linear m vs. applied voltage from benchtop tests

These values enter the control map through (26) once B is rotated into the body frame via the chosen attitude parametrization (see Sec. III-B) and after applying per–axis current limits to model saturation in the QP. Validation details and the measurement setup are as reported in the source study.

VI. Control Architecture, Synthesis, and Analysis

This section fixes the complete control pipeline for nadir-pointing with magnetorquers using a receding-horizon CLF–QP, provides a block diagram, and analyzes controllability, observability, and stability. I use the modeling from Secs. III–V (notably (15), (20), (21)–(25)). Hardware limits follow the characterized magnetorquer in [10]; attitude/frames and rigid-body dynamics follow [1]; magnetic-control properties follow [2]; the CLF–QP construction follows [9].

a) It is to be again duly noted that a known limitation of magnetorquers are their inability to actuate in a direction parallel to earth's magnetic field due to θ (angle between magnetic field and magnetorquer coil) being Zero, making the system underactuated. However, this is not a dead-end, we can still take control of the satellite in all directions by exploiting the time-varying orbit geometry to eventually gain control in all axes.:

A. Signal definitions and pipeline

At sample k:

1) Build the horizon $\{q_{d,k}\}_{k=0}^{N}$ from LVLH/ECI (Sec. IV).
2) Estimate $(\hat{q}_k, \hat{\omega}_k)$ from $\tilde{\omega}, \tilde{b}_{\mathcal{B}}$ (MEKF).
3) Compute $B_{\mathcal{B},k} = C(\hat{q}_k) B_{\mathcal{I}}(t_k)$.
4) Linearize to obtain A_k, B_k, c_k as in (15).
5) Form the CLF inequality (20) using $\tilde{q}_k, \tilde{\omega}_k$.
6) Solve (21)–(25) for $m_0^\star$; map to currents and saturate.
7) Step the plant; shift the horizon; repeat.

B. Transfer-function considerations

The plant is nonlinear and time-varying because $B_{\mathcal{B}}(t) = C(q)B_{\mathcal{I}}(t)$ depends on attitude and the orbit. A single SISO transfer function is therefore not appropriate. A small-angle linearization about a *fixed* $B_{\mathcal{B}}$ yields

$$\theta = \omega, \quad \omega = -I^{-1}[B_{\mathcal{B}}]_\times \, m,$$

which is a double-integrator with direction-dependent input matrix. This is useful only for sanity checks. I therefore do not incorporate classical transfer functions in the synthesis; for I do not have the required knowledge of how to incoperate such a SISO system with and imply Lyuapunov guarentees to it. All design uses the CLF-QP with the time-varying magnetic channel [1], [2].

C. Controllability and reachability

Instantaneously,

$$\tau_{\text{mtq}} = m \times B_{\mathcal{B}} = -[B_{\mathcal{B}}]_\times m, \quad \operatorname{rank}([B_{\mathcal{B}}]_\times) = 2 \ (B_{\mathcal{B}} \neq 0),$$

so torque is confined to the plane orthogonal to $B_{\mathcal{B}}$ and the instantaneous input matrix $G(t) = I^{-1}(-[B_{\mathcal{B}}(t)]_\times)$ has rank 2. Over an orbit, $B_{\mathcal{B}}(t)$ varies in direction; for the linearized time-varying system

$$x_{k+1} = A_k x_k + B_k m_k, \quad B_k = \begin{bmatrix} 0 \\ -I^{-1}[B_{\mathcal{B},k}]_\times \end{bmatrix} \Delta t,$$

the controllability Gramian

$$W(t_0, t_1) = \int_{t_0}^{t_1} \Phi(t_1, \tau) B(\tau) B(\tau)^\top \Phi(t_1, \tau)^\top d\tau$$

is full rank when $B_{\mathcal{B}}(\tau)$ spans three independent directions on $[t_0, t_1]$. Thus, magnetorquer-only control is effectively 3-axis controllable in a *time-varying* sense for generic LEO, provided the prediction window covers sufficient field rotation [2]. Feasibility under saturation: $\|\tau\|_{\max} \leq \|m\|_{\max} \|B_{\mathcal{B}}\|$. With the characterized coil ($200 \times 200 \times 10\,\text{mm}$, $n = 250$, $S = 3.497 \times 10^{-2}\,\text{m}^2$, $i_{\max} \approx 0.92\,\text{A} \Rightarrow m_{\max} \approx 8.19\,\text{A m}^2$) and typical LEO $\|B\| \sim 20$–$60\,\mu\text{T}$, peak torques are $\mathcal{O}(10^{-4})\,\text{N m}$ [10]. I choose $N, \alpha, \kappa, Q, \lambda$ so the demanded contraction in (20) is compatible with these limits.

D. Observability and estimation

Measurements are

$$y_k = \begin{bmatrix} \tilde{\omega}_k \\ \tilde{b}_{\mathcal{B},k} \end{bmatrix} = \begin{bmatrix} \omega_k \\ C(q_k) b_{\mathcal{I}}(t_k) \end{bmatrix} + \begin{bmatrix} \eta_{\omega,k} \\ \eta_{b,k} \end{bmatrix}.$$

A single magnetic vector does not determine attitude instantaneously, but along an orbit $b_{\mathcal{I}}(t)$ and hence $b_{\mathcal{B}}(t)$ vary in direction. With gyro kinematics, the time-varying pair (A_k, C_k) becomes observable over typical LEO windows (persistently exciting). I therefore use a MEKF to provide $(\hat{q}, \hat{\omega})$ to the controller [1]. Bias states can be included if required.

E. Stability analysis (CLF–QP closed loop)

With

$$V(x) = \tfrac{1}{2}\, \omega^\top I \omega + \tfrac{\kappa}{2} \|\tilde{q}_v\|^2,$$

the per-stage inequality (20)

$$(B_{\mathcal{B}} \times \omega)^\top m \leq -\alpha V - \tfrac{\kappa \tilde{q}_0}{2} \tilde{q}_v^\top \omega + \delta$$

is affine in m and enforces an upper bound on $\dot{V}$. If $\delta = 0$, $\dot{V} \leq -\alpha V$ gives exponential decay $V(t) \leq e^{-\alpha t} V(0)$. With $\delta \geq 0$ and a quadratic penalty in (21), the closed loop is *practically* exponentially stable to a ball whose radius scales with the worst-case slack (and with bounded disturbances/noises acts as an ISS-type bound). Embedding this inequality at each horizon stage preserves convexity and yields the receding-horizon CLF–QP used here [9]. In implementation I monitor $\delta_k^\star$ (Fig. VI-0a) as a certificate of feasibility margin.

F. Implementation notes for evaluation

I explicitly log $\|m\|_\infty$, $\|i\|_\infty$, $\delta_k^\star$, and the angle-to-nadir error. I also plot the direction of $B_{\mathcal{B}}(t)$ across each horizon to support the controllability discussion and include disturbance and sensor-noise sweeps to report robustness.

Appendix: State-Space for LQR/MPC Baselines

Linearize about $(\tilde{q}, \boldsymbol{\omega}) = (0, 0)$ and nominal $\mathbf{B}_b(t)$ to obtain

$$\delta \dot{x} = A(t)\, \delta x + B(t)\, \delta \mathbf{m},$$

with periodic A, B. Design TVLQR or discrete-time MPC with input bounds; compare against CLF–QP in identical scenarios.

Appendix: Assumptions and Parameters

Assume: principal axes alignment, bounded $\|\boldsymbol{\tau}_d\|$, known orbit and $q_d(t)$, estimator provides $(q, \boldsymbol{\omega})$ at ≥ 10 Hz, and $\mathbf{B}$ from IGRF/dipole model. Typical $m_{\max} = 0.2\,\text{A m}^2$; tune $(\kappa, \alpha, p, \lambda)$ empirically.

REFERENCES

[1] T. J. D. Ruiter, C. J. Damaren, and J. R. Forbes, *Spacecraft Dynamics and Control: An Introduction*. Chichester: John Wiley & Sons, 2013.

[2] S. Silani and M. Lovera, "Magnetic spacecraft attitude control: A survey and some new results," *Control Engineering Practice*, vol. 13, no. 3, pp. 357–371, 2005.

[3] M. L. Psiaki, "Magnetic torquer attitude control via asymptotic periodic lqr," *Journal of Guidance, Control, and Dynamics*, vol. 24, no. 2, pp. 386–394, 2001.

[4] R. Wisniewski, "Linear time-varying approach to satellite attitude control using magnetic torquers," *Journal of Guidance, Control, and Dynamics*, vol. 22, no. 6, pp. 849–857, 1999.

[5] P. Wang, Y. Shtessel, and Y. Wang, "Satellite attitude control using only magnetorquers," in *IEEE Aerospace Conference*, 1998.

[6] T. Miyata and J. van der Ha, "Attitude control by magnetic torquer for small satellite," in *AAS/AIAA Space Flight Mechanics Meeting*, no. AAS 09-169. American Astronautical Society, 2009.

[7] M. J. Sidi, *Spacecraft Dynamics and Control: A Practical Engineering Approach*. Cambridge University Press, 1997.

[8] P. C. Hughes, *Spacecraft Attitude Dynamics*. Mineola, NY: Dover Publications, 2004, unabridged republication of the 1986 Wiley edition.

[9] A. D. Ames, X. Xu, J. W. Grizzle, and P. Tabuada, "Control barrier function based quadratic programs for safety critical systems," *IEEE Transactions on Automatic Control*, vol. 62, no. 8, pp. 3861–3876, 2017.

[10] T. Panyalert, S. Manuthasna, J. Chaisakulsurin, T. Masri, K. Palee, P. Prasit, P. Torteeka, and P. Konghuayrob, "Characterization and verification of the optimal feedback gain of a satellite magnetorquer-based attitude control system," *Advances in Space Research*, vol. 74, no. 11, pp. 5745–5766, 2024. [Online]. Available: https://www.sciencedirect.com/science/article/pii/S0273117724008664